



universität
wien

A large-area beam telescope using extremely fine-pitched Silicon detectors

Author
Alina WEISER

Supervisor
Uwe KRÄMER

September 6, 2017

Abstract

The most popular infrastructure requests at the DESY Testbeam facility are beam telescopes for reference position and momentum measurements. Currently there is an ongoing project developing a new large area silicon beam telescope at the DESY Testbeam. Different tests are conducted on this setup. Measurements are performed on the electrical properties of the sensors and on the performance of the readout chip and DAQ. This includes calibration, tests with a radioactive source and testbeam measurements. Tests of the sensors show good electrical behaviour and they were shipped to IZM for bump-bonding. The full synchronisation of the KP1X readout and the testbeam was achieved.

Contents

1. Introduction	3
1.1. The DESY Testbeam Facility	3
2. Theory	4
2.1. Silicon Sensors	4
2.1.1. The p-n Junction	4
2.1.2. Semiconductors as Detectors	6
3. Silicon Strip Detectors for the DESY Testbeam	7
3.1. Measurements	8
3.1.1. Apparatus and Methodology	8
3.1.2. IV-Setup	9
3.1.3. CV-Setup	9
3.2. Results and Analysis	10
3.2.1. IV-Measurements	10
3.2.2. CV-Measurements	11
3.2.3. Visual Inspection of the quality of the sensors	11
3.2.4. Measurements of a wire-bonded test-structure	12
4. KPiX	14
4.1. General Measurement Setup	15
4.2. Calibration Measurements and Noise Runs	16
4.2.1. Results	17
4.3. Measurements with the ⁹⁰ Sr-Source	19
4.3.1. Results	20
4.4. The Testbeam Setup	21
4.5. Measurements at the Testbeam	22
4.5.1. Results	22
5. Conclusion and Outlook	27
6. Acknowledgements	28
Appendices	28
A. Acronyms	28

1. Introduction

1.1. The DESY Testbeam Facility

The DESY testbeam facility, which can be seen in figure 1 provides three beam lines (21, 22 and 24) where research and development of detectors can be conducted.

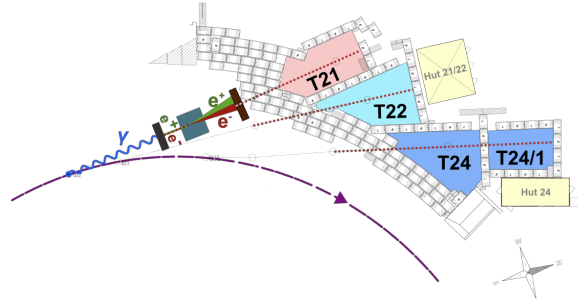


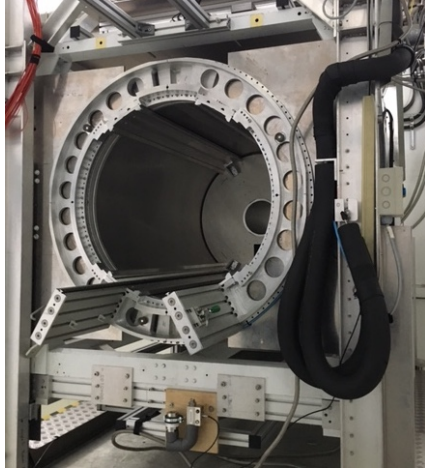
Figure 1: DESY Testbeam Facility [2]

The beam is provided by the DESY II accelerator, which is a electron-positron synchrotron with an average radius of 46.6 m. It mainly operates as an injector for DORIS and PETRA but the bremsstrahlung created in it, is used for the Testbeam facility.

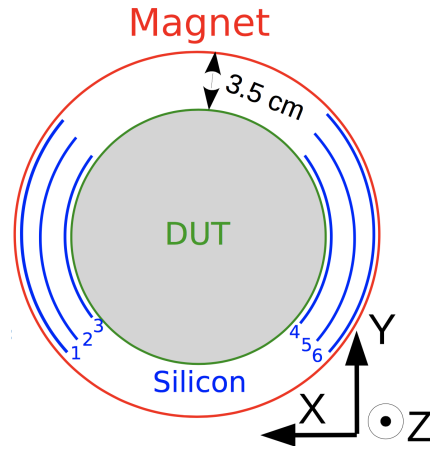
The bremsstrahlung beam is generated by a carbon fibre target in the circulating beam of the synchrotron DESY. The photons are then converted to electron/positron pairs with a metal plate (converter). After that the beam is spread out into a horizontal fan with a dipole magnet. The final beam is sliced out of this fan with a collimator.

This e^+e^- -beam can provide up to 1000 particles per cm^2 with an energies ranging from 1 GeV to 6 GeV. [2] Along the three beam lines there are four test areas. Testbeam area T21 is equipped with a dipole magnet, and T24/1 with a superconducting solenoid called PCMAG. With 83% of the users wanting to use an external silicon telescope it is by far the most popular infrastructure request. Two of the testbeam areas T21 and T22 are already equipped with small sized $1 \times 2 \text{ cm}^2$ eudet-style pixel beam telescopes. [3] A large area silicon telescope has been requested to accompany to the PCMAG.. The PCMAG which can be seen in figure 2(a) has $\sim 75 \text{ cm}$ of usable inner diameter, however since most of this space is covered by the device under test, only $\sim 3.5 \text{ cm}$ are available on each side for the silicon telescope. A beam telescope used within the magnetic field should have at least five layers of silicon because one would need that for the reconstruction of a helix path. It should also have a spatial resolution better than $10 \mu\text{m}$ in the plane of the track. This is mostly driven by the spatial resolution needed for a Time Projection Chamber (TPC) prototype used as a DUT.

To fulfil this large number of user requests and the requirements for such this kind of telescope, a large area silicon strip telescope will be built consisting of three layers of silicon sensors on each side of the tested devices. A schematic overview of the setup can be seen in figure 2(b).



(a) PCMAG in testbeam area T24/1



(b) Schematic overview of silicon telescope inside the PCMAG

Figure 2: The superconducting PCMAG

2. Theory

2.1. Silicon Sensors

Due to their electric characteristics such as conductivity, Semiconductors such as Silicon can be used as particle detectors. The conductivity can be influenced by introducing impurities into the material, which is called doping. There are two possibilities for doping, called n-type and p-type doping.

For p-type doping of a semiconductor, atoms with one valence electron less than the basic semiconductor material are added. Those atoms with a lower main chemical group act as electron acceptors. On the other hand, to get a n-type semiconductor atoms with one valence electron more are introduced. In this case, the atoms are from a higher main chemical group and act as electron donors.

For silicon (Main group IV), a material mainly used for detectors, one would introduce an element of group III like boron to receive a p-type semiconductor and a element of group V like phosphorus for a n-type.

2.1.1. The p-n Junction

The Junction also called Diode is the merging of a p-doped material and a n-doped one. Since on both sides of the junction there is a different concentration of charge carriers, the electrons of the n-doped material diffuse into the p-type material where they recombine with holes. On the other hand, holes from the p-type material diffuse into the n-doped one where they also recombine with electrons. The result of this reaction is the development of a region that is free of any free charge carriers, the so called depletion

tion region. The p-doped region is charged negatively and the n-doped one positively which results in a electric field that stops the complete diffusion process.

External voltage can be applied to the Diode in two directions, the forward bias mode and the backward bias mode shown in figure 3.

1. **forward bias mode:** If the positive pole is connected to the p-type side and the negative pole is applied to the n-type semiconductor, the p-n Junction is called forward biased. As a result of the applied voltage the potential barrier is reduced and the depletion zone narrows down until it disappears causing a large direct current.
2. **reverse bias mode:** Converse to the forward bias mode, the positive pole is connected to the n-type and the negative-pole is connected to the p-type semiconductor. If voltage is applied, the potential barrier and with it, the depletion zone will increase. However, in this bias mode there is a small leakage current, because charge carriers can still be thermally excited in the depletion zone. Therefore this leakage current is also strongly dependent on the temperature. If the reverse bias voltage becomes too great, the electric field strength will also increase and cause the Diode to break down and the current to increase exponentially.

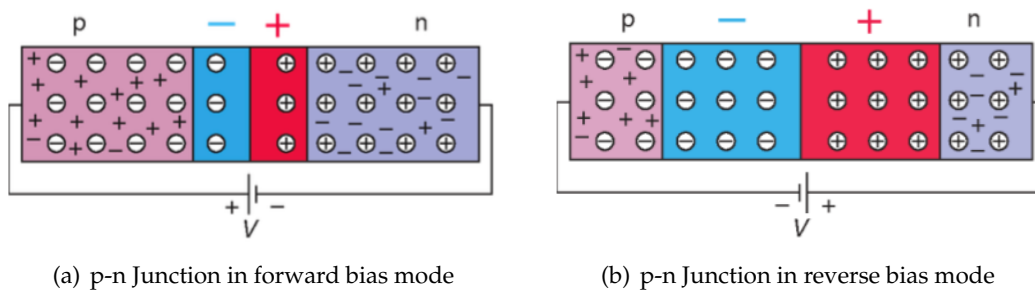


Figure 3: Shift of the depletion zone depending on the biasing method, Source:[6]

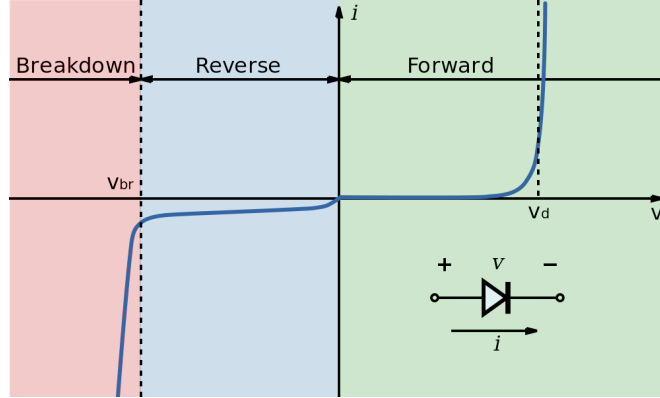


Figure 4: Characteristic curve of a p-n Junction [4]

The Figure 4 shows the characteristic curve of a p-n-Junction for both the forward bias mode, which can be seen on the positive x-axis and the reverse bias mode on the negative x-axis.

Because of its charge carrier free depletion zone, a p-n Junction can be seen as a parallel plate condensator filled with a dielectric, where the non-depleted area corresponds to the capacitor plates and the depleted area corresponds to the dielectric.

If the p-n Junction is operated in reverse bias mode, then an increase in voltage will lead to an increase in the width of the depletion zone and therefore a decrease of the capacitance. The capacitance will continue to decrease until the depletion zone has propagated over the entire semiconductor. After this point, a further increase in external voltage will not lead to an additional decrease of capacitance. [5]

The voltage at full depletion V_{depl} can consequently be deduced by plotting $\frac{1}{C^2}$ versus the Voltage V .

2.1.2. Semiconductors as Detectors

A semiconductor detector is basically a fully depleted reverse biased p-n Junction. The real operating voltage is however almost always chosen slightly higher than V_{depl} , this is called over-depletion. Because of the backwards bias mode the leakage current which is dominated by thermally generated e^-h^+ -pairs is relevant. Due to the applied electric field those generated pairs can not recombine but rather they are separated and drift to the electrodes causing the leakage current.

The depleted zone of the detector is sensitive to incoming charged particles. Those particles loose a fraction of their energy because of the interaction with matter. This energy deposition leads to a production of electron hole pairs along its path in the depletion zone. Those pairs are then separated by the applied external electric field and drift towards the electrodes causing a measurable electric current.

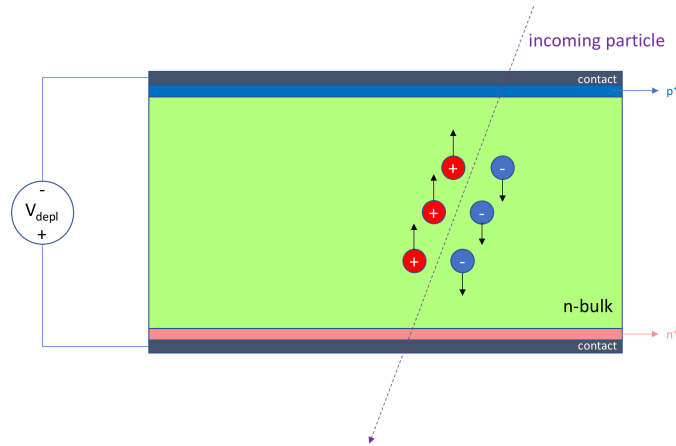


Figure 5: Particle Sensor principle: Created electron-hole pairs drift to opposite directions because of the electric field and create a current

If multiple diodes operated in reverse bias are combined together and multiple of those detectors are stacked in several layers, a 3 dimensional recreation of a particle track can be achieved.

3. Silicon Strip Detectors for the DESY Testbeam

The Silicon sensors chosen for the construction of the silicon telescope for the Testbeam were designed by the Stanford Linear Accelerator Center (SLAC) for the planned Silicon Detector (SiD) in the future International Linear Collider (ILC). They are Silicon Strip Detectors (SSD) with a strip pitch of $25\ \mu\text{m}$. Every second strip is going to be read out, while the other strips encourage charge sharing which has a positive effect on the resolution of the sensor. With a thickness of $320\ \mu\text{m}$ and an active area of $10 \times 10\ \text{cm}^2$ they fulfil all the requirements for the beam telescope.

Figure 6 shows the silicon strip sensors used for the future telescope. One of the read-out chips is bump-bonded to the surface of the sensor. The readout cable wire-bonded to the sensor.

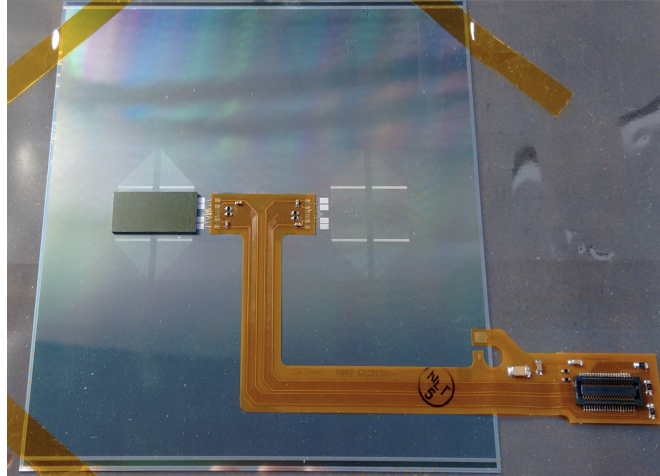


Figure 6: Silicon strip sensor with bump-bonded KPiX readout chip and wire-bonded readout cable.

3.1. Measurements

The SSD for the Testbeam just arrived from their manufacturer Hamamatsu and are not bump bonded to the chip and wire bonded to the readout cable yet, they will be tested in a probe station.

The electrical properties of the sensors were measured in a clean room. Current-Voltage (IV) Measurements were conducted to determine the overall behaviour and stability of the sensors. Capacitance-Voltage (CV) Measurements were also performed to determine the depletion voltage of each of the sensors.

3.1.1. Apparatus and Methodology

Figure 7 shows the equipment used for the measurement as well as the probe station. The following devices were used:

1. **Keithley High Voltage (HV) Supply:** This voltage supply was used to apply the bias voltage to the backside of the sensor.
2. **IV-CV Measuring Unit (LCR) Meter:** This LCR unit measured both the capacitance and the current flowing through the bias ring which the probe was connected to.
3. **IV-CV Switch:** This is used to switch the internal electronics of the LCR Meter so that either IV and CV measurements can be taken by the same device.
4. **Keithley Picoammeter:** High Precision Ammeter to measure the current.

5. **PC:** Both the High Voltage Source and the LCR Meter are connected to the PC. The IV and CV measurements are initiated and controlled with a program which also stores the data into a txt. file.
6. **Probe Station:** The probe station contains a circular chuck with vacuum support. When the sensor is placed on top, the HV can be applied to the backside. The needles are installed in probes that can move in 3 axes. There is also a microscope to help with the precise positioning. The entire probe station is contained inside a darkbox to decrease the light induced noise.

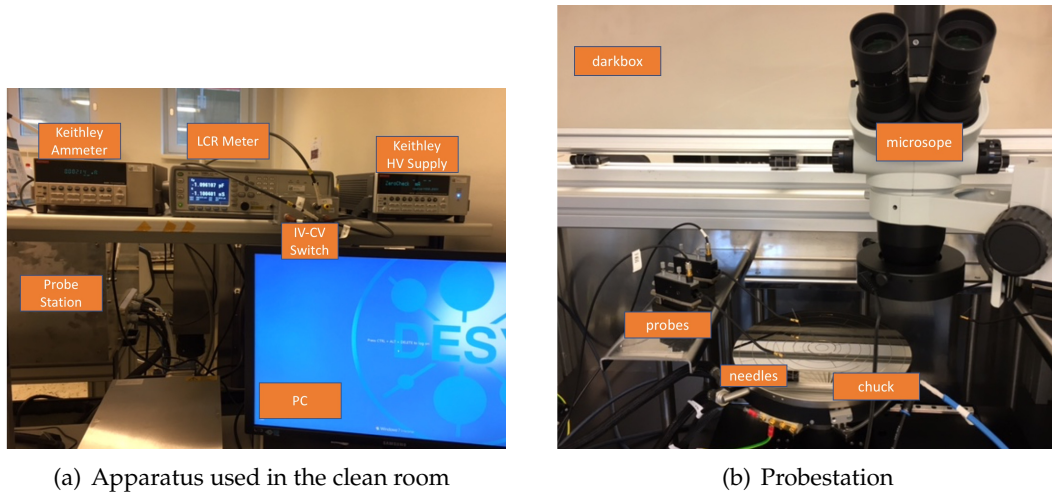


Figure 7: Equipment used to measure the electrical properties of the sensors

3.1.2. IV-Setup

To measure the current with respect to the bias-voltage one of the bias ring pads is contacted with a needle. This is done with the help of a microscope and a probe that can move in x,y and z direction. The backside is biased with the high voltage and the needle is connected to the ammeter to measure the current. The ammeter is also connected to the PC through the LCR Meter with the IV-CV switch. The current was measured for up to 300V bias voltage. The setup of the system can be found in figure 8(a).

3.1.3. CV-Setup

To measure the capacitance two probe needles are contacted to two different bias ring pads. Again high voltage is applied to the backside of the sensor. Capacitance-Voltage measurements were also conducted up to a bias voltage of 300V. The setup of the system can be found in figure 8(b).

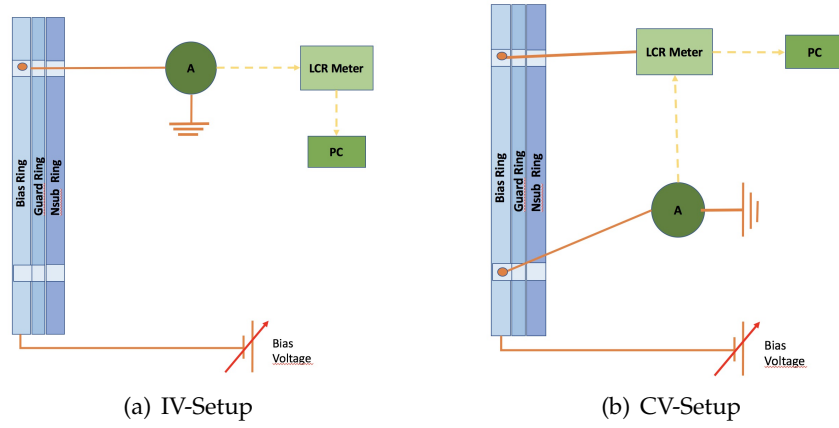


Figure 8: Schematic overview of the IV and CV measurement setup

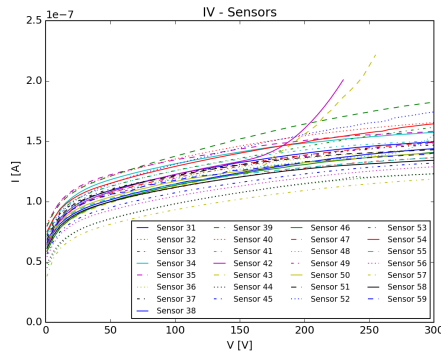
3.2. Results and Analysis

The following section will cover the results obtained by the measurements conducted and described in 3.1.

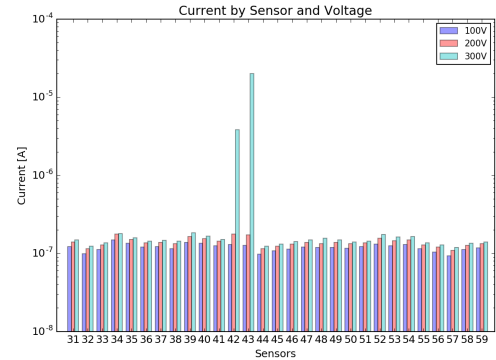
To analyse the data taken in the IV and CV measurement-runs multiple python scripts were used.

3.2.1. IV-Measurements

The following plot 9(a) shows the measured current for applied bias voltages up to 300V for each of the 29 sensors.



(a) measured IV curve for all silicon sensors



(b) Voltage at 100V, 200V and 300V for each sensor

Figure 9: Results for the current, voltage measurements

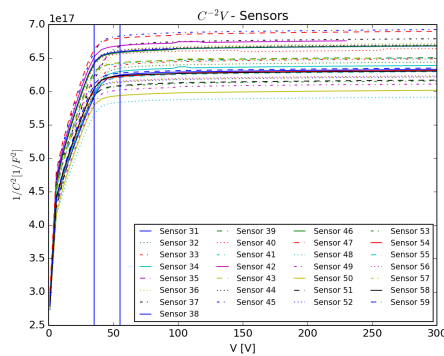
27 out of the 29 measured sensors are stable until 300 V and show the expected be-

haviour with low leakage currents in the nA range. Two of the sensors 42 and 43 reach the breakdown voltage at around 250 V. Figure 9(b) shows a diagram with all the sensors on the x axis, the current is plotted on the y axis for at three different voltage levels. It can be seen that the current increases exponentially for the two sensors that break through prior to 300 V. The fact that those two sensors break down early however does not affect the project since the sensors are going to be operated a little over-depleted at around 50 V as shown in subsection 3.2.2.

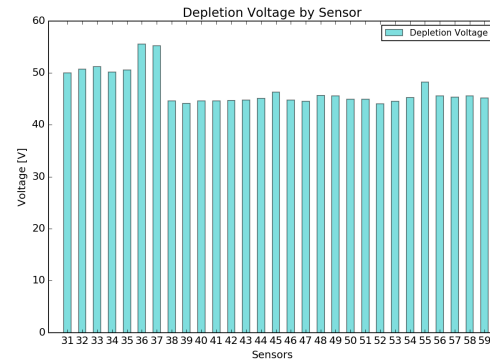
3.2.2. CV-Measurements

The following figure 10(a) shows $\frac{1}{C^2}$ versus voltage measurements. As mentioned in 2.1.1 by plotting this, the depletion voltage can be obtained. The typical behaviour for a working silicon detector can be observed here. The capacitance decreases with the voltage until the sensor is fully depleted due to the growth of the depletion zone. Once the sensor is fully depleted the capacitance stays constant. The zone where the sensors reach the full depletion voltage is indicated by two blue lines in figure 10(a).

Figure 10(b) shows a block diagram of each sensors depletion voltage. It can be observed that the depletion voltage for each of the sensors is between 45 V and 55 V. This is the good behaviour expected from the sensors and confirms that they can be operated at around 50 – 60 V.



(a) measured $\frac{1}{C^2}$ versus depletion voltage for all 29 sensors



(b) Depletion voltage for each of the sensors

Figure 10: Results for the capacitance, voltage measurements

3.2.3. Visual Inspection of the quality of the sensors

Additionally to the measurements of the electrical properties of the sensors, visual inspections of all the sensors were conducted. For this, a VHX microscope was used to check for any imperfections on the surface of the sensors such as scratches, chemical residues or other marks.

It was observed that all sensors were in pristine condition with one exception, a sensor

that had multiple scratches and chemical marks. This imperfect sensor 51 however still showed very good electrical properties.

Figure 11 shows one of those scratches damaging seven strips.

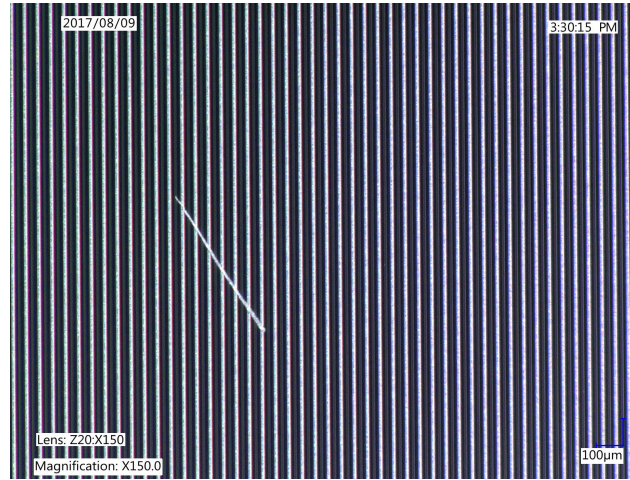


Figure 11: Scratch on the strips of sensor 51

3.2.4. Measurements of a wire-bonded test-structure

Additionally to all the measurements mentioned above, one of the test-structures was sent to a wire-bonding lab at DESY and tested prior to wire-bonding and after, to see if the intended wire-bonding technique damages the sensor. After wire-bonding, the test-structure was glued to two layers of gold-plated PCB. Because high voltage could not be applied to the backside anymore, the IV-measurement was conducted with two needles. One needle contacted the Nsub Pad, which has an internal connection to the n doted layer on the backside of the sensor, and applied high voltage. This needle replaced the high voltage normally applied through the chuck. The other needle contacted the bias ring pad to measure the current. The setup of this measurement can be seen in figure 12.

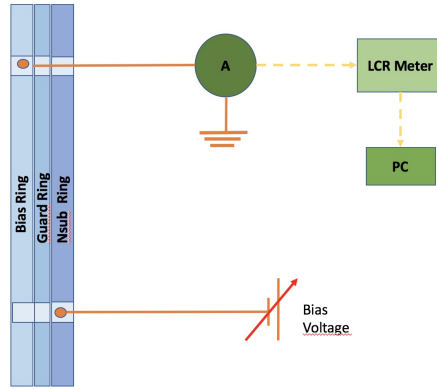
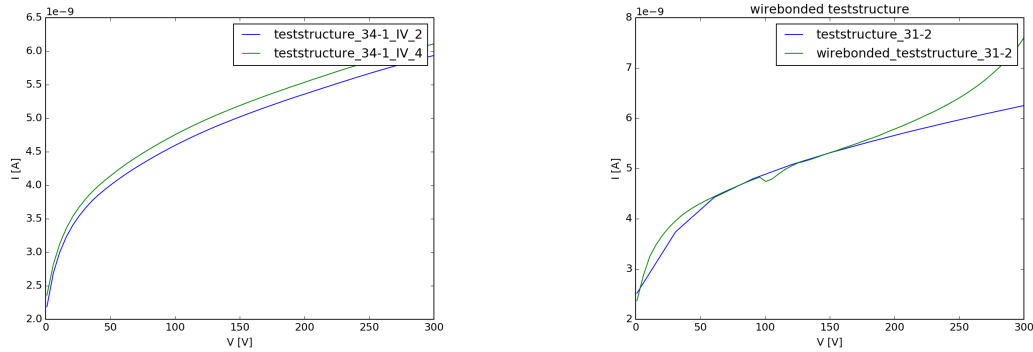


Figure 12: Schematic overview of setup for IV measurement with the wire-bonded teststructure

To check whether or not it made a difference if the high voltage is applied to the back-side of the test-structure or the Nsub pad, both measurement techniques were conducted on a test-structure. The difference in current for the two tests is ~ 0.2 nA, which is not significant for the measurement and can therefore be neglected. The result of this measurement can be found in subfigure 13(a).



(a) IV measurements conducted with teststructure 34-1; blue: HV applied to the backside; green: HV applied to the Nsub pad

(b) IV measurements for teststructure 31-2 before and after wirebonding

Figure 13: Results for the capacitance, voltage measurements

In subfigure 13(b) the IV-measurement conducted prior to wire-bonding and the one performed after are plotted. It can be observed that the currents for both measurements are the same until 200 V. After that the wire-bonded teststructure shows a soft breakdown. This could be due to possible damages on the sensors surface caused by wire-bonding and pull-tests that were conducted. However no visible imperfections such as scratches were observed with the microscope.

4. KP iX

Another important part of the detector are the readout electronics.

KPiX is a 1024 Channel Readout System on a Chip, which is intended to be bump bonded directly on various large area silicon sensors. KPiX was also developed by SLAC for the SiD intended for the ILC. Because of the beam structure of the ILC, KPiX runs in Acquisition Cycles shown in figure 14. It is only active for a short time span and deactivated the rest of the time.

One Acquisition Cycle consists of a start up phase of $\sim 1\text{ms}$, followed of the data taking time, a data storing time of $\sim 1\text{ms}$ and finally a read out time of $\sim 20\text{ms}$. The chip can then be turned off for a desired amount of time.

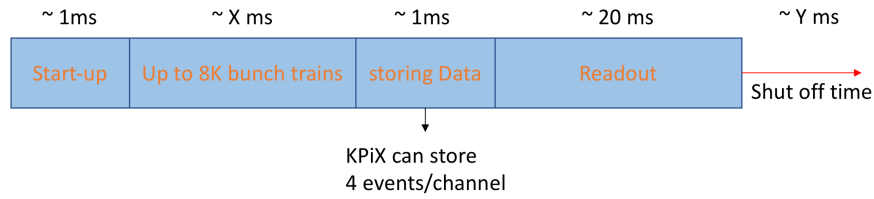


Figure 14: Acquisition Cycle of the KPiX chip

Due to this "power pulsing" the chip can save about a factor of 100 in power consumption. [1]

KPiX contains an integrated pitch adapter and has a calibration system for each of the readout channels. For this, the chip can induce a varied amount of charge to the channel. A simplified block diagram of a single KPiX readout channel can be seen in figure 15. Each of the channels consists of a dynamically switchable gain charge amplifier, shaping, threshold discrimination, 4 sample and hold capacitors and 4 timing registers. The chip can therefore register 4 separate measurements of time and amplitude of threshold crossing during each bunch train. [1]

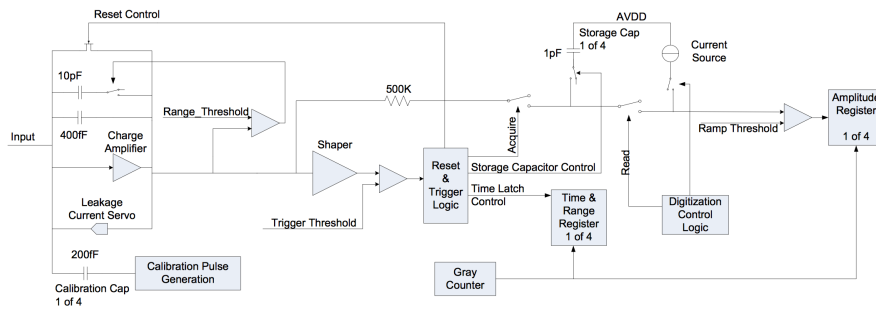


Figure 15: Simplified block diagram of a single KPiX readout channel [1]

KPiX can work in two modes:

1. **Internal Trigger Mode:** This self trigger mode requires a certain threshold. Any event exceeding this threshold will be registered. In this mode, KPiX can store 4 events per acquisition cycle per channel.
2. **External Trigger Mode:** On the other hand KPiX also allows for a forced or external trigger mode. If an external trigger signal is recorded, every channel of the sensor stores the current state. In this mode, KPiX can store 4 events per cycle.

4.1. General Measurement Setup

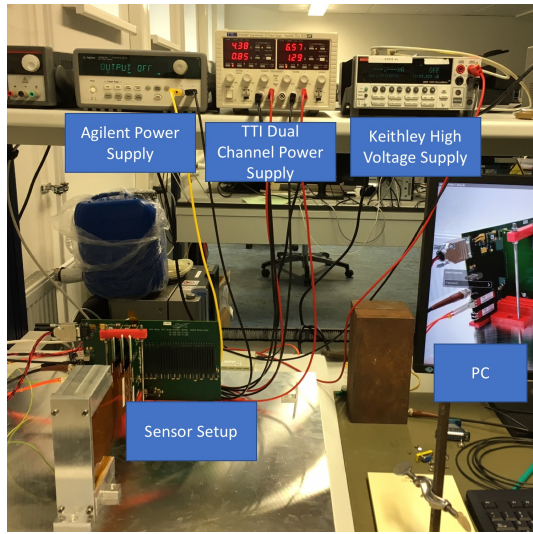
To measure and test the performance of the KPiX chip, three silicon electromagnetic calorimeter sensors were used that have been bump bonded to a KPiX chip. The sensors are connected through wirebonded Kapton cables to Frontend-cards, which are connected to a DAQ Board with a powerful Field Programmable Gate Array (FPGA). The sensors and DAQ board are mounted in a holding structure.

To reduce light induced noise during the measurements a darkbox is put over the sensors and the DAQ board. In addition, the holding structure and the darkbox are grounded to reduce electromagnetic noise. Through a small hole in this cover, the DAQ Board is connected to four different power supplies providing voltage to the KPiX, the sensor and the FPGA. The DAQ board is also connected to the PC via an optical fibre cable. The PC starts and controls the entire measurement process with the help of a GUI. This GUI is used to build up a connection between the PC, the FPGA on the DAQ board and the KPiX chip. Due to this, the run state and settings of the KPiX can be controlled. The configurations are set with different xml files for the corresponding measurements conducted. The xml files can change arguments like thresholds, active channels, acquisition cycles and much more.

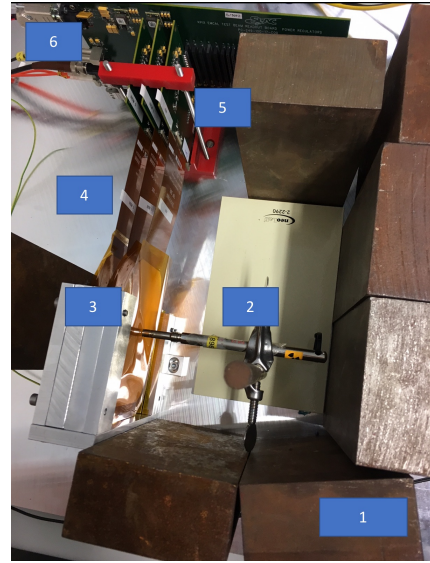
For the measurements conducted using a radioactive source, a special holding structure is used to hold the source in the wanted position. In this case multiple iron blocks (1) are also set up in order to shield from any harmful radiation. During the measurements, the following equipment was used:

1. **TTI Dual Channel Power Supply:** This power supply delivered two different voltages. First voltage for the analog part of the KPiX chip which was kept constant at a value of 4.37 V. It additionally provided the necessary 6.57 V for the FPGA.
2. **Agilent Power Supply:** The Agilent delivered a voltage of 4.14 V needed for the digital part of the KPiX readout chip.
3. **Keithley High Voltage Supply (HV):** Lastly this high voltage supply provided the bias voltage for the silicon sensors. A voltage of 50V was used in order to fully deplete the sensors.

The entire setup of the measurements conducted with the KPiX is shown in figure 16. The general overview with all voltage supplies can be found in subfigure 16(a). Subfigure 16(b) shows a closeup of the setup inside the darkbox for measurements with a radioactive source.



(a) Entire setup with Voltage Supplies



(b) Closeup of the sensor setup used for measurements with the radioactive source: (1) radiation shielding; (2) radioactive source; (3) ECal sensors; (4) Kapton cables; (5) Frontendcards; (6) DAQ board

Figure 16: Setup for measurements with the KPiX chip

For the measurements with the radioactive source, a beta radiating Strontium-90 source was used, because it radiates highly energetic electrons of ~ 2.2 MeV. This is really important because less energetic particles are absorbed even in a thin layer of silicon and would not reach the last sensor.

4.2. Calibration Measurements and Noise Runs

Since the KPiX chip measures ADC counts, the corresponding charge is calculated with the help of calibration measurements. For this the KPiX induces the sensors with certain amount of charge and measures the corresponding ADC count. To do this, the "running calibration" mode was used in the GUI interface and the corresponding xml configuration file was chosen. For the noise runs, a normal background only measurement using internal triggering was conducted using the "running" mode in the GUI. With this measurement noisy channels were identified, as well as the threshold with which to run the experiments with a source or a beam.

Figure 17 shows a screenshot of the GUI interface that was used for the measurements.

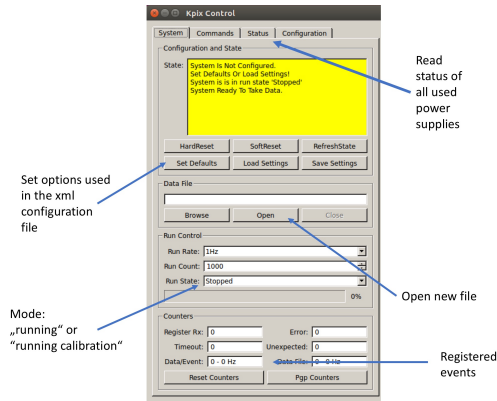


Figure 17: Screenshot of GUI interface

4.2.1. Results

The following section will cover all the results obtained by the calibration measurements and noise runs with the KPiX readout chip. To receive the plots, C++ and root scripts were used. Those scripts were also used for the analysis for all other measurements conducted with the KPiX.

As mentioned in 4.2 the goal of the calibration measurements was to find the corresponding charge to each ADC count. The following figure 18(a) shows good calibration behaviour of a channel in sensor 30. Sub-figure 18(b) however shows the behaviour of a "dead channel". For this channel no matter how much charge is by the chip, the chip always measures the same amount of ADC counts.

Figure 18(c) shows the slope acquired for each channel of each sensor plotted into a histogram. There is a small amount of channels around 0 that show this bad behaviour where the channels do not respond to the charge injection.

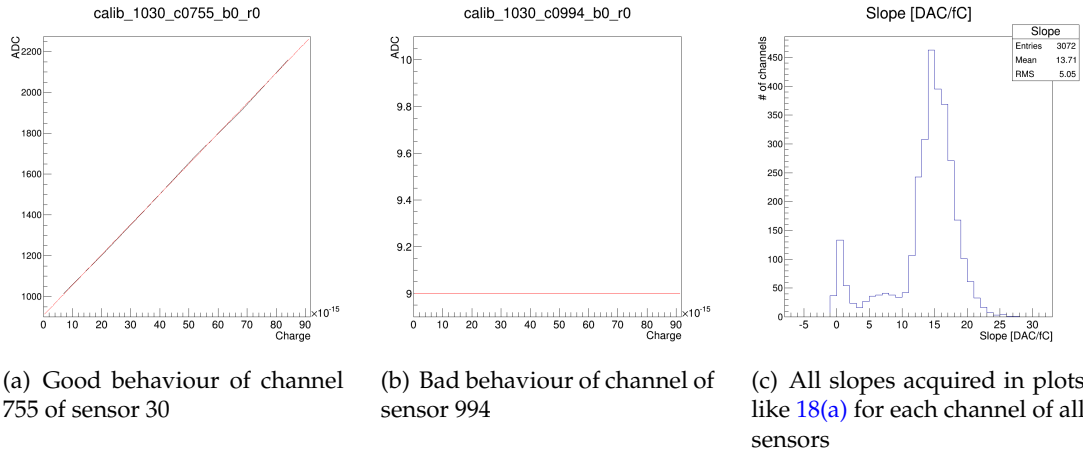
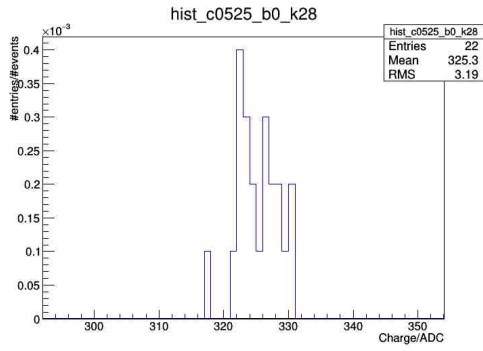


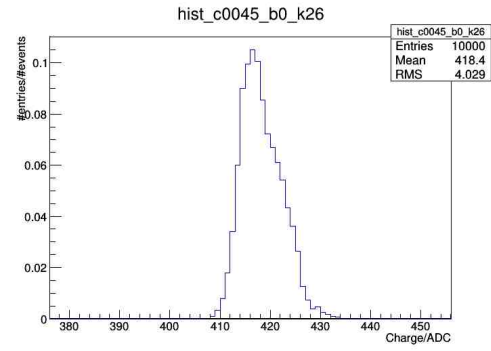
Figure 18: Calibration measurement results

Those "dead" channels were deactivated manually for any future measurements since they do not deliver a correct signal or result.

The noise runs were mostly used to find any noisy channels, channels that fire too often even though there are no actual particles going through the sensor. It is really important to deactivate those channels so they can not affect the surrounding channels in a bad way and causing the entire sensor to malfunction. For the following results, measurements with 10.000 acquisition cycles were taken. In the following figure 19, a working channel and a noisy channel is shown. In subplot 19(a) the histogram of a channel that is working well is plotted. It shows that this channel recorded 22 noise events in 10.000 acquisition cycles. The sub-figure on the right side 19(b) however shows a very noisy channel. This channel triggered 10.000 times, that means, that each time the sensor was able to measure something, this channel measured an event even though there was nothing there.



(a) histogram of channel with good behaviour



(b) Noisy channel

Figure 19: Comparison between a channel with good behaviour and a noisy channel

The channels that did not show any calibration response and the noisy channels differ from sensor to sensor and were deactivated for each of the sensors respectively. The following figure 20 shows the sensor map for sensor 26. In red one can see the activated channels, whereas the channels in dark blue have been deactivated for the reasons mentioned above. Out of the working channels around 3% showed either of the problems mentioned above.

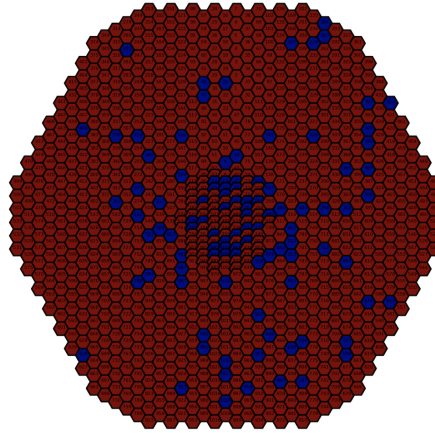


Figure 20: Channel Map for sensor 26; active channels are shown in red, deactivated channels are shown in blue

4.3. Measurements with the ^{90}Sr -Source

The ^{90}Sr -Source was mounted on the holding structure and the iron blocks were set up for radiation shielding. The measurements were conducted in the same way as the background run using internal triggering and the "running" mode in the GUI. Two sensors were operated at a threshold of 240 and one at a threshold of 235. This was due

to the fact that the last sensor was a lot noisier. It should be noted that threshold 240 is actually a lower threshold than 235. (A threshold of 255 is the 0 point any number lower than that corresponds to a threshold higher than 0) These measurements were conducted to see whether or not the entire setup works together. This includes the configuration files and software as well as the hardware. In specific preparation for the testbeam it was important to investigate if the impact of a source could actually be seen and measured by the system.

4.3.1. Results

The following figure 21 shows the plotted sensor maps for the measurement with the Strontium-90 source.

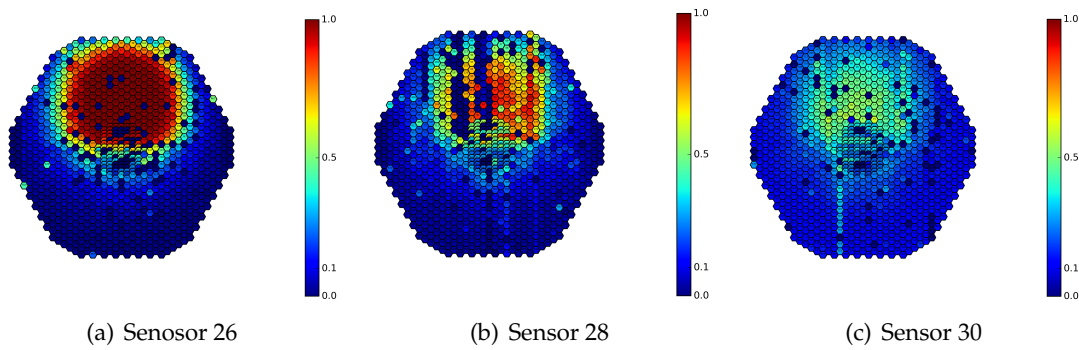


Figure 21: Sensor maps for all three sensors using a ^{90}Sr -Source and internal triggering; Colours show the entries/acquisition cycles

The sensors were arranged the following way. Sensor 26 was closest to the source, 28 in the middle and 30 the farthest away. This can be seen in figure 22.

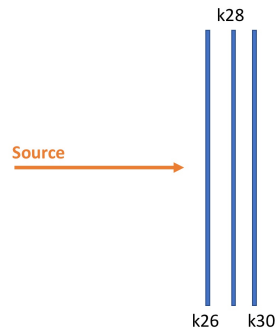


Figure 22: Sensor order for the source measurement

The resulting sensor maps show the expected behaviour for such a setup when using a radioactive ^{90}Sr -Source. The sensor closest to the source shows a large circular spot be-

cause of the electrons emitted by the Strontium Source. The electrons then get absorbed by each layer of silicon and decrease strongly with the distance. The dark blue channels in the radiated spot (especially the dark blue lines on sensor 28) have been deactivated due to reasons mentioned in section 4.2.1.

4.4. The Testbeam Setup

The Testbeam setup can be seen in the following figure 23.

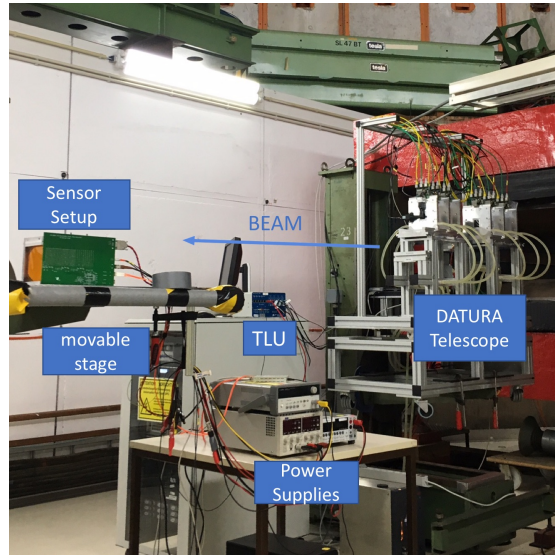


Figure 23: Setup of devices in the Testbeam area

To test the chips even further and check if they work fully synchronised to the DESY II accelerator cycle, measurements were also conducted at the DESY Testbeam Area T21. For this the entire general setup was taken to the testbeam area. The sensors were mounted on a movable stage and were moved into and aligned with the beam. Additionally to the normal setup the DATURA telescope was used for external triggering as well as saving timestamps. For this, the signal of all four scintillators was routed to a Trigger Logic Unit (TLU). The coincidence Nuclear Instrumentation Standard (NIM)-signal of this TLU was then led to the hut via a patch panel to be converted into a Transistor-transistor logic (TTL)-signal with the help of a Level Adapter NIM-crate. The signal was then wired back through the patch panel to the Testbeam area so it could be connected to the DAQ Board.

The DESY Testbeam provides the TTL minimum energy signal, which was used to synchronise the KPiX chip to the DESY II cycle. Firstly this signal was converted into a NIM signal with a Level Adapter. In order to synchronize the system, this signal was then delayed with a Gate and Delay Generator before being lead through the patch panel to the DAQ board.

Since for the measurement 4 GeV electrons were used, this delay was set to 25 μ s. For

the different beam energies a different delay has to be used, since the signals differ in length. The measurements concerning this delay were already conducted during the last testbeam measurements.

4.5. Measurements at the Testbeam

The following measurements were conducted at the Testbeam:

The internal trigger and external trigger measurements were conducted both synchronized and unsynchronized to the beam. For each of the different measurements, 10.000 acquisition cycles were measured. There are two collimators used to focus the beam. For the internal trigger measurements the size of the two collimators was varied, resulting in 4 different collimator options. (collimator inside: $7 \times 7 \text{ mm}^2$ and $15 \times 15 \text{ mm}^2$, collimator outside: ± 5 and ± 10). The collimator inside was changed manually by switching out the two respective ones. The collimator outside the testbeam area was opened and closed via a control panel in the hut.

1. **Internal Trigger:** The measurements were conducted like the measurements with the Strontium-90 source. The thresholds used for this measurements were again 240 for sensor 28 and 30 and 235 for sensor 26.
2. **External Trigger:** The DATURA telescope was used as a force trigger. Every time all four scintillators triggered in a small time frame the kpix triggered all the channels on each sensor, to "make a picture of the current state of the sensor".
3. **Angle Measurement:** For this measurement the sensors were rotated in the y direction in reference to the beam. After the rotation of the system, a normal measurement with internal trigger was conducted synchronized to the beam.
4. **Threshold-scan:** For this at each threshold ranging from 255 to 220 a noise run was conducted, followed by a normal measurement run with the beam. Measurements were taken in steps of 5.

4.5.1. Results

The sensor order was kept the same from the measurements with the radioactive source. The successful integration into the DESY II accelerator cycle can be best shown with the sensor maps obtained by the external trigger measurements. The following plots [24](#) show the sensor maps for sensor 26 on the one hand unsynchronized to the testbeam and on the other side synchronized to the system.

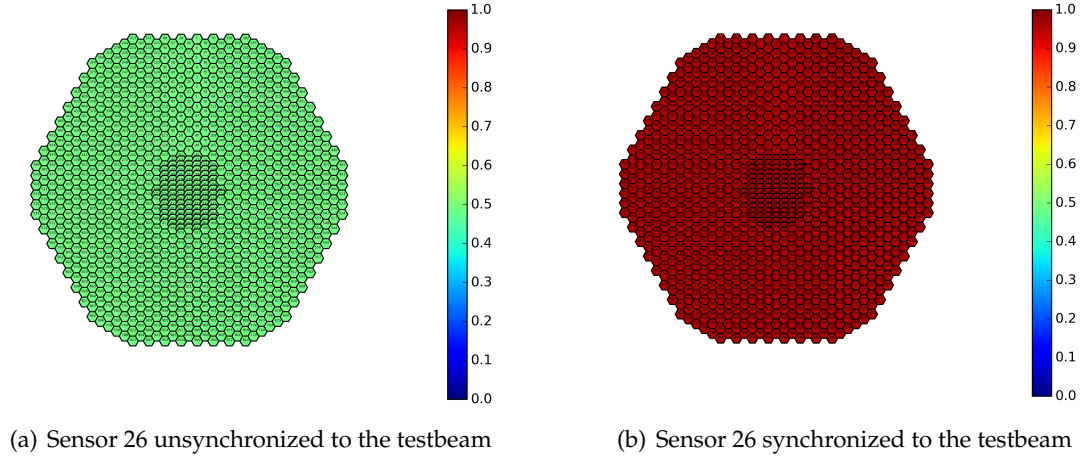


Figure 24: Comparison between unsynchronized and synchronized system using external triggering; Plots show the amount of triggers/acquisition cycles

The reason why the sensors are fully evenly coloured is because the maps show the amount of triggers divided by the amount of measured acquisition cycles. Since in the external trigger mode every channel triggers when the DATURA telescope gives a coincidence signal each channel of the sensor is the same colour.

However what can be seen by the colour differences between the two different measurements is that the sensor that was synchronized to the testbeam cycle triggers in every acquisition cycle. That means every single time the sensor was ready to measure there were actually particles from the beam. The sensor unsynchronized to the DESY II cycle however does not trigger every single time, since there are no particles there at certain times and therefore the DATURA telescope does not send a coincidence signal to trigger.

The internal trigger measurements were conducted both with a system aligned with the beam and with a setup that was rotated on the y direction. The following plot shows the sensor maps for the setup rotated in y direction in reference to the beam. The schematic view of this alignment can be seen in figure 25.

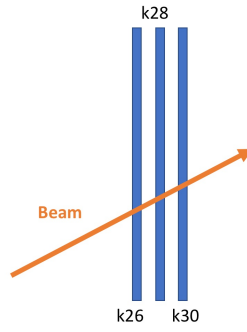


Figure 25: Sensor order for the rotated testbeam measurement

The sensor maps obtained by the angle measurement are shown in the following figure 26. Firstly the difference between the testbeam and the measurement with the source, shown in figure 21, that can be observed very clearly here is that the electrons of the beam used had an energy of 4 GeV in comparison to the electrons emitted by the Strontium source which had an energy of around 2.2 MeV. Whereas in the measurement with the source the electrons get absorbed by the silicon due to their low energies, in the testbeam they just pass through. The same amount of particles that can be observed in sensor 26 can also be seen in sensor 30.

At this point it should be mentioned again that the sensors were operated with different thresholds (a higher threshold for the old sensor 26, and lower thresholds for the newer sensors 28 and 30). The reason why it looks like there were more particles in the last sensor (30) than the first one (26) was just due to the fact that the threshold was lower for sensor 30.

The collimator used for the experiments has a square shape but because of the distance to the detectors one would expect a circular beamspot on the sensors. What can also be observed in the rotated measurement is that the beamspot rather than being circular has an elongated shape due to the fact that the beam is going through the sensor with an angle. That means that the distance that the particles have to travel through the sensor (in y direction) is longer, resulting in an elongated beamspot.

The beamspot also moves through the sensors, rather than staying on the same place in each one of them.

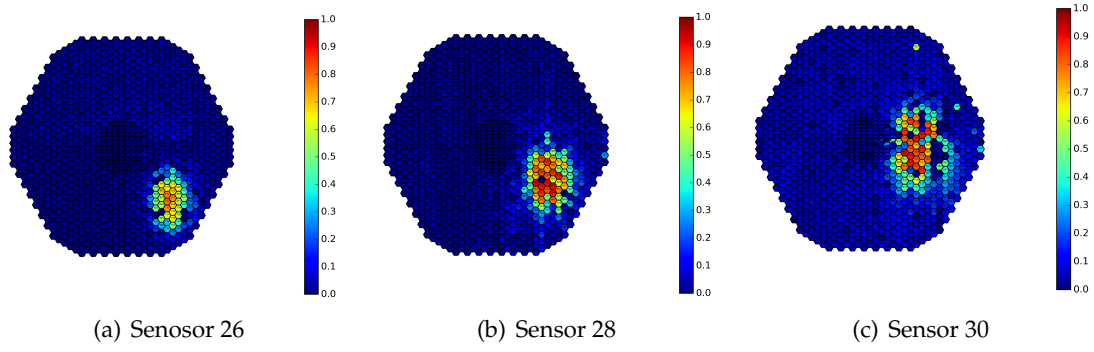


Figure 26: Sensor maps for all three sensors in the testbeam, using internal triggers; The system was positioned with an angle relative to the beam direction; Colours show the entries/acquisition cycles

Electrons loose their energy in thin layers of silicon according to a Landau distribution. This behaviour was also checked in the results obtained from the angle measurement. The following figure 29 shows the amount of entries/events per charge deposited. The result was fit with a landau distribution.

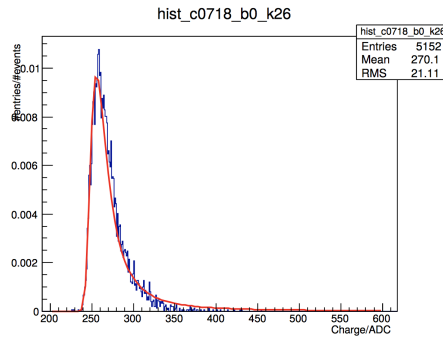


Figure 27: Entries/events per charge deposited in ADC counts

The landau fits reasonably well to the obtained data. The reason for the strong increase of entries at 240 ADC is that there was a threshold set for this measurement. If any particle passed through and deposited less charge, the KPiX chip simply did not trigger.

Additionally correlation plots were created for the angle measurement, to see whether or not the data obtained by the different sensors actually correlates. The resulting correlation maps can be seen in figure 28

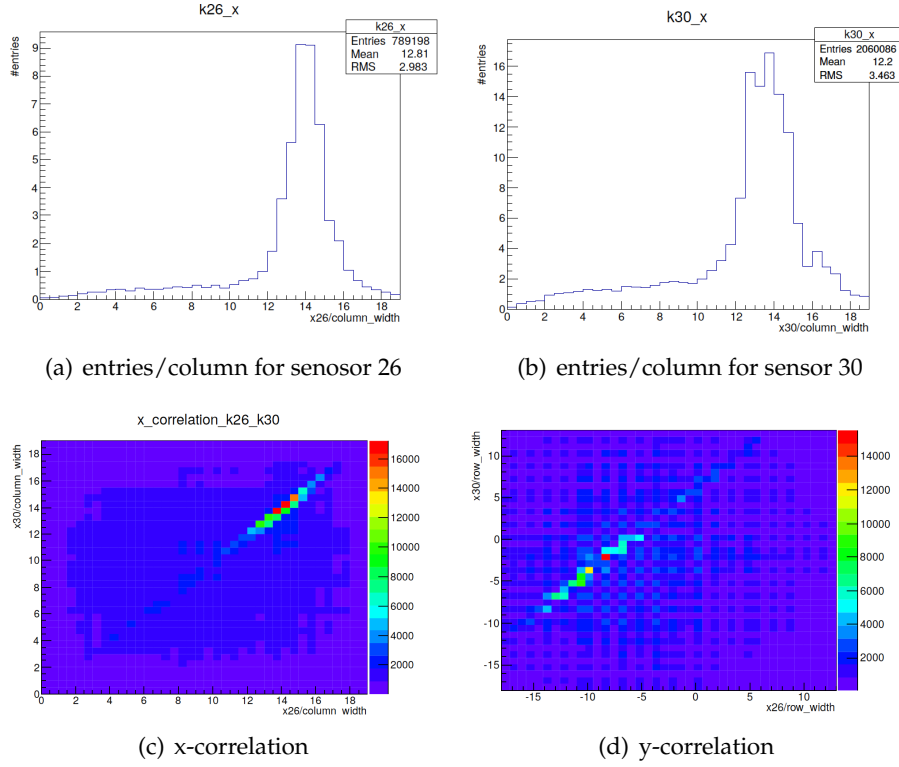


Figure 28: Correlation plots for sensor 26 and 30 for the angle measurement using internal triggers

To create the correlation plots the measured entries were plotted against the column width of the sensor. This was done for both the x- and y-axis of the sensors. In subfigure 28(a) the entries over the column width are plotted for the x-direction and sensor 26. Subfigure 28(b) shows the same for sensor 30. Then, in a correlation plot which can be seen in subfigure 28(c), the results of both sensor 26 (plotted on the x-axis) and sensor 30 (plotted on the y-axis) were combined. The same thing was done for the y-direction of the sensors, the resulting correlation plot can be seen in subfigure 28(d).

One can observe that the sensors are perfectly correlated in the x direction, where there is a maximum at 14 for sensor 26 there is also a maximum for sensor 30. This correlation is indicated by the green/red line in the x-correlation plot. On the other hand there is still a correlation y direction of the sensors, however this time this correlation is shifted. Where there is a maximum for sensor 26 at a column width of -10, it is at -5 for sensor 30. This is due to the angular rotation in the y direction in reference to the beam.

Lastly, a threshold scan was conducted with beam using internal triggers. The following plot shows the entries/events over the KPiX channels for four different thresholds for all three sensors.

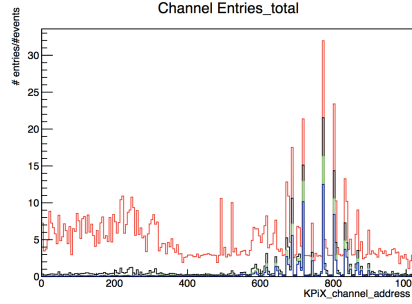


Figure 29: Entries/events per KPiX channel address; red: threshold 250, black: threshold 240; green: threshold 230; blue: threshold 220

The beam is located around KPiX channel address 600-900. The threshold of 250 shows significant noise in the channels where the beam does not hit the sensor. The threshold of 240 already decreases this noise to almost zero. The noise is not decreased a lot more by the higher thresholds 230 and 220, however the signal is decreased by those thresholds.

5. Conclusion and Outlook

In conclusion, the silicon strip sensors that were produced by Hamamatsu were all in good condition and behaved accordingly.

The sensors were therefore sent to IZM for bump bonding to the KPiX chips. They will be delivered back to DESY where the readout cable will be wire-bonded onto the sensor.

To be sure that the wire-bonding technique does not damage the sensors, additional teststructures should be sent to the wire-bonding lab in order to measure the impact this procedure has on the sensor.

To test the KPiX chip they were first calibrated. Noise runs and measurements using a radioactive Strontium-90 source were conducted in preparation for testbeam measurements. Full synchronisation of the KPiX readout chip to the DESY II cycle was achieved. A first analysis of the testbeam data showed that the entire setup operated successfully. Further analysis should be performed for validation.

After the strip sensors are fully assembled (KPiX chip and readout cable are bonded to the sensor) additional testing should be done, to check the performance of the system with the [SSD](#).

The ultimate goal of this project is the installation of the final Assembly into a working telescope at DESY Testbeam. The target date for completion is April 2018.

6. Acknowledgements

First and foremost, I would like to thank my supervisor Uwe Krämer for his invaluable help, assistance and support during my time here at DESY. I would also like to thank Dr. Marcel Stanitzki, Dr. Mengqing Wu and Dr. Dimitra Tsionou for always giving a helping hand, answering all my questions as well as helping me with coding problems and presentations. Lastly I would like to thank the entire FLC TPC group for making this an invaluable, unforgettable and very enjoyable experience.

Appendices

A. Acronyms

SLAC Stanford Linear Accelerator Center

ILC International Linear Collider

SiD Silicon Detector

SSD Silicon Strip Detectors

ECAL Electromagnetic Calorimeter

HCAL Hadronic Calorimeter

FPGA Field Programmable Gate Array

TLU Trigger Logic Unit

NIM Nuclear Instrumentation Standard

TTL Transistor–transistor logic

TPC Time Projection Chamber

References

- [1] J Brau, M Breidenbach, A Dragone, G Fields, R Frey, D Freytag, M Freytag, C Gallagher, G Haller, R Herbst, et al. Kpix-a 1,024 channel readout asic for the ilc. In *Nuclear Science Symposium and Medical Imaging Conference (NSS/MIC), 2012 IEEE*, pages 1857–1860. IEEE, 2012.
- [2] DESY. Test Beams at DESY. <http://particle-physics.desy.de/e252106/>.
- [3] Wojciech Dulinski. Tapi: High precision beam telescope based on mimosa-18 monolithic pixel sensor and tnt2 data acquisition boards. *EUDET-Memo-2008-22*, 2008.

- [4] Electronics. Diodes. <http://pakistanelectronics.blogspot.de/2010/04/diodes.html>.
- [5] Hermann Kolanoski and Norbert Wermes. *Teilchendetektoren*. Operations Research, 2016.
- [6] Manfred Krammer. Silicon detectors. Institute of High Energy Physics, Vienna, 2010/11.